Scientific Research Publishing

Open Journal of Geology, 2024, 14, 126-141
https://www.scirp.org/journal/ojg
ISSN Online: 2161-7589
ISSN Print: 2161-7570

Petrographic and Geochemical Characteristics of the Pouni Palaeoproterozoic Formations North of the Léo Square Degree (Burkina Faso, West Africa)

Adama Ouédraogo Yaméogo[1,2*], Pascal Ouiya[2,3], Hubert Gounwendmanaghré Zongo[2,4], Omar Akonyiré[2], Abraham Seydoux Traoré[2], Saga Sawadogo[2], Séta Naba[2]

[1]Unité de Formation et de Recherche en Sciences et Technologies, Département des Sciences de la Vie et de la Terre, Université Norbert Zongo, Koudougou, Burkina Faso
[2]Unité de Formation et de Recherche en Sciences de la Vie et de la Terre, Laboratoire Géosciences et Environnement (LaGE), Département des Sciences de la Terre, Université Joseph Ki-Zerbo, Ouaga, Burkina Faso
[3]Ecole Normale Supérieure (ENS), Institut des Sciences et de Technologie (IST), Ouaga, Burkina Faso
[4]Ecole Supérieure d'Ingénieries, Université de Fada N'gourma, Fada N'Gourma, Burkina Faso
Email: *ayameogofr@yahoo.fr

How to cite this paper: Yaméogo, A.O., Ouiya, P., Zongo, H.G., Akonyiré, O., Traoré, A.S., Sawadogo, S. and Naba, S. (2024) Petrographic and Geochemical Characteristics of the Pouni Palaeoproterozoic Formations North of the Léo Square Degree (Burkina Faso, West Africa). *Open Journal of Geology*, **14**, 126-141.
https://doi.org/10.4236/ojg.2024.141008

Received: December 25, 2023
Accepted: January 27, 2024
Published: January 30, 2024

Abstract

The Pouni area is made up of basalts belonging to the Boromo belt, lamprophyres and granitoids. These geological formations are similar to geological formations of the same type in other regions of the Palaeoproterozoic domain of the Man/Leo shield. This study, which focused on the petrographic and geochemical characteristics of these geological formations, led to the following main conclusions: The lamprophyres are basic plutonic rocks that cut through other geological formations. The basalt belongs to the northern part of the Borormo belt and is thought to be a relic of overthickened oceanic plateaus. There are two groups of granitoid rocks. The granodiorite has a geochemical signature close to that of Archean TTGs and is metaluminous in character. It has a low potassium content. The minor element and rare earth element spectra indicate that it could be derived from partial melting of basic magmatic rocks. Biotite granites are peraluminous and highly potassic. Minor element contents and rare earth spectra indicate that they could be derived from partial melting of felsic materials. Geotectonic diagrams show that the granitoids identified in the Pouni zone were emplaced in an active tectonic context, similar to that of present-day subduction zones.

Keywords

Burkina Faso, Dori, Man/Léo Shield, Petrography, Geochemistry, Partial Melting, Geotectonic Context

1. Introduction

The central-western part of Burkina Faso, like the rest of the country and the Baule-Mossi region (**Figure 1**), consists of Paleoproterozoic (~2 Ga) terrains containing metasediments, metavolcanites and granitoids [1] [2] [3]. The latter were emplaced during the Eburnian orogeny and are very good markers of crustal deformation. A distinction is made between early or first generation granitoids with an affinity to Archean TTGs, second generation granitoids which are calc-alkaline-potassic and late granitoids which are alkaline. In the Baoulé-Mossi area, studies of TTG-type granitoids and calc-alkaline granitoids have helped to define their petrogeochemical characteristics and the geodynamic contexts in which they were emplaced during the Eburnian orogeny [1] [2] [4] [5] [6]. It has been suggested that TTG-type granitoids are derived from partial melting of greenstone and are emplaced in a subduction context. For biotite granites or calc-alkaline granitoids, partial melting of both metabasic lower crust and TTG-type granitoids has been proposed in a volcanic arc context [1] [2]. It is also proposed that the crustal protoliths, heated by the underlying magmas, were partially melted in an Archean tectonic style without collision [7] [8].

This study focuses on the belt formations and granitoids in the commune of Pouni in the province of Sanguié, Burkina Faso (**Figure 2**). The aim of this study is to define the mineralogical and geochemical compositions of these belt formations and the mapped granitoids in order to constrain the geodynamic processes that prevailed during emplacement of these formations. At the field scale, the biotite granites are very poorly structured. In a forthcoming study, we plan to use the Anisotropy of Magnetic Susceptibility (AMS) technique to highlight the internal structures of these granitoids in order to better constrain their emplacement process.

2. Geological Setting

The study area is located near the Boromo belt, in central western Burkina Faso, between 2.47˚W and 2.63˚W longitude and between 11.83˚N and 12.05˚N latitude (**Figure 2**). This belt is mainly composed of basalts and andesites, with a few intercalations of sediments and basic plutons [9] [10]. The Boromo greenstone belt is intruded by TTG-type granitoids. After the latter emplacement, the greenstone belt and TTG granitoids were intruded by highly potassic calc-alkaline granitoids [1].

In the study area, granitoids outcrop west of the village of Pouni and near the village of Tita. Granodiorites, biotite granites and porphyritic biotite granites can be observed. As part of the 1/1,000,000 mapping of Burkina Faso, Castaing *et al.*, (2003) [1] indicates the presence of a leucogranite at Pouni.

3. Methodology

We used a sampling grid with a maximum spacing of one kilometre, as long as outcrop conditions allowed, and the samples collected at each station were

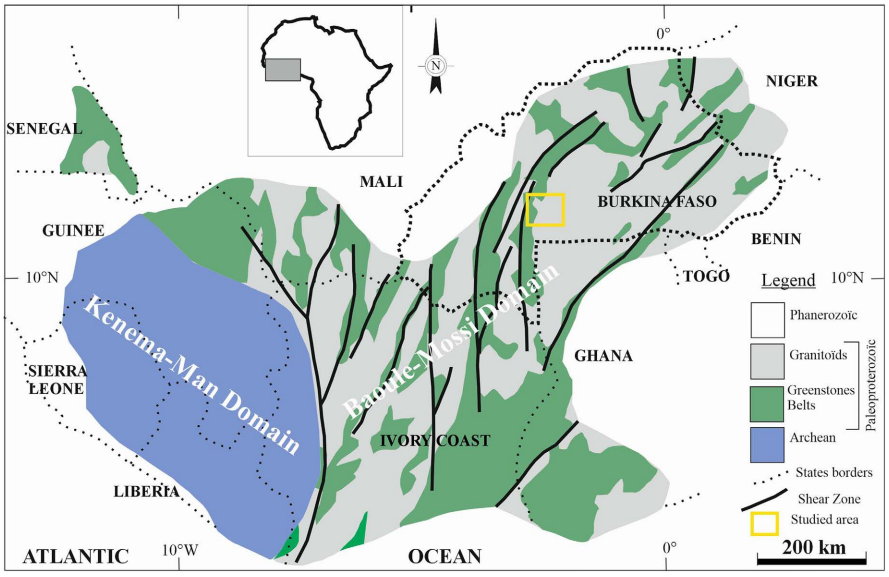

Figure 1. Position of the synthetic geological map of Burkina Faso on the Man/Leo shield.

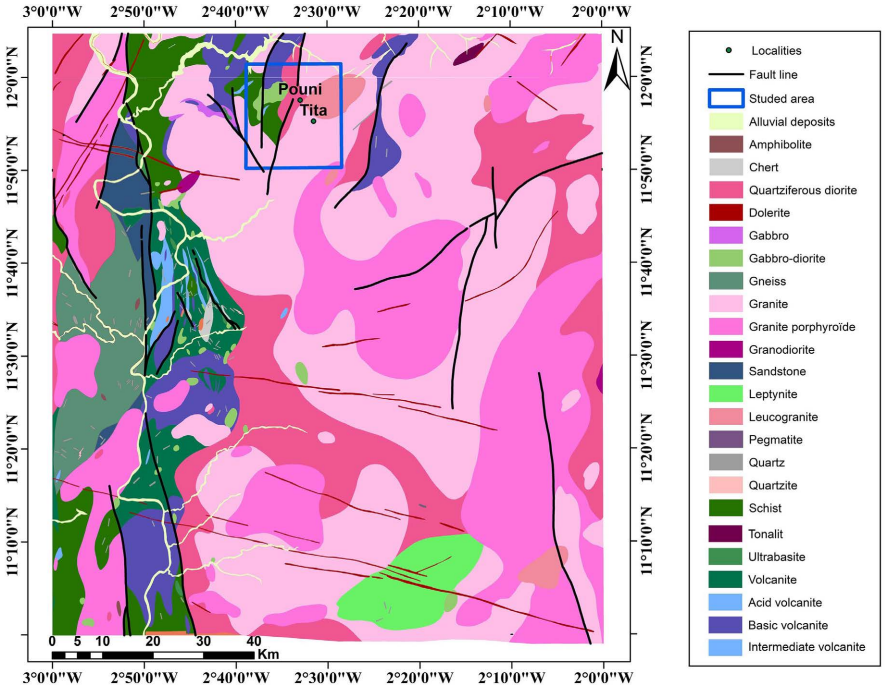

Figure 2. Position of the study area on the Léo square degree geological map.

described. In the laboratory, twelve (12) thin sections were prepared and examined under a polarising microscope. The selection of samples for whole rock geochemical analysis was guided by the variations in mineralogical composition that appeared during the microscopic observations. A total of six (06) samples were analysed, including one (01) basalt sample, one (01) lamprophyre sample, one (01) granodiorite sample and three (03) biotite-granite samples. The whole rock geochemical analyses were carried out at the ALS laboratory in Ireland,

which was responsible for all the various sample preparations prior to analysis by ICP-MS and ICP-AES. Information on the methods used by the ALS laboratory is available at https://www.alsglobal.com.

4. Results

4.1. Petrography of Belt Rocks

The study area covered a small part of the Boromo belt near the village of Pouni (**Figure 2**). The outcropping rocks are mainly basalts and lamprophyres.

- **Basalts**

Basalts are massive and dark (**Figure 3(a)**). They outcrop in the form of small hills containing boulders or clusters of boulders. Macroscopic observation shows that basalt is aphyric. Microscopically (**Figure 3(b)**), the basalt consists almost entirely of amphibole, in the process of destabilisation into actinote or chlorite. Small amounts of biotite, plagioclase and quartz islands can be seen. The sample observed under the microscope is criss-crossed with quartz-plagioclase veinlets.

- **Lamprophyres**

Lamprophyres are dark coloured rocks (**Figure 4(a)**). In the field they occur as small boulders or clusters of boulders. Microscopically, lamprophyres are composed mainly of plagioclase, pyroxene and amphibole. The amphiboles are altered to muscovite. Opaque colours are associated with ferromagnesian minerals.

4.2. Petrography of Granitoids

- **Granodiorites**

The granodiorite is light in colour and medium to slightly coarse grained (**Figure 5(a)**). The visited outcrops have no measurable structures. Microscopically (**Figure 5(c)**), the white minerals are predominantly plagioclase, followed by quartz. Potassium feldspars, represented by microcline, are present in small amounts. The ferromagnesian minerals are biotite and amphibole. Biotite is slightly more common than amphibole. Auxiliary minerals include epidote, zircon and opaque.

- **Le granite à biotite**

It is a very poorly structured rock with biotite as the only ferromagnesian mineral. Biotite granite is leucocratic and the texture is essentially medium grained (**Figure 5(b)**). Microscopically (**Figure 5(d)**), biotite granite is composed of straight quartz, plagioclase and potassic feldspar. The other white minerals are plagioclase and potassium feldspar in more or less equal proportions. Accessory minerals are mainly sphene, zircon, epidote and a few opaques.

4.3. Geochemistry of Rocks in the Study Area

4.3.1. Basalt and Lamprophyre

Les résultats des analyses géochimiques indiquent des teneurs en silice comprise entre 50% et 52 % (**Table 1**). Dans le diagramme ternaire AFM de [11] (**Figure 6**),

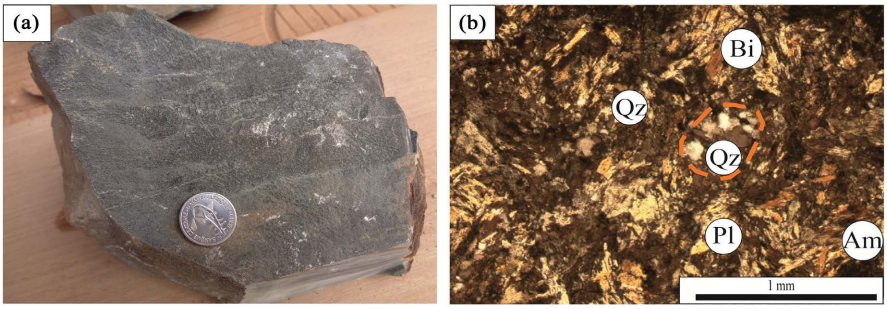

Figure 3. Macroscopic and microscopic view of the basalt: (a) Basalt sample; (b) Microphotograph showing the average mineralogical composition of the basalt (polarised and analysed light): Am: Amphibole, Bi: Biotite, Pl: Plagioclase, Qz: Quartz.

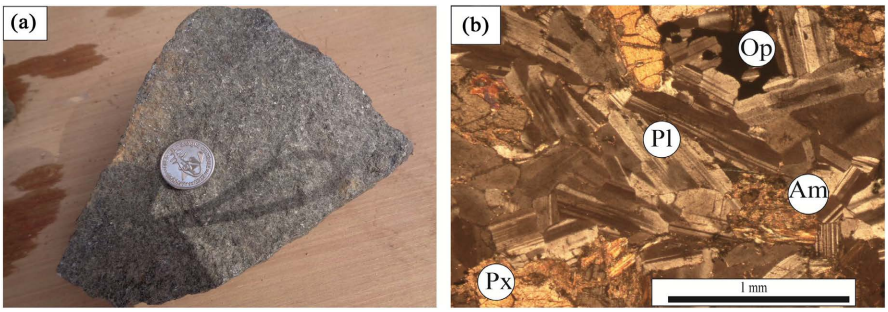

Figure 4. Macroscopic and microscopic view of lamprophyre: (a) Lamprophyre sample; (b) Microphotograph showing the average mineralogical composition of lamprophyre (polarised and analysed light): Px: Pyroxene, Am: Amphibole, Pl: Plagioclase, Op: Opaque.

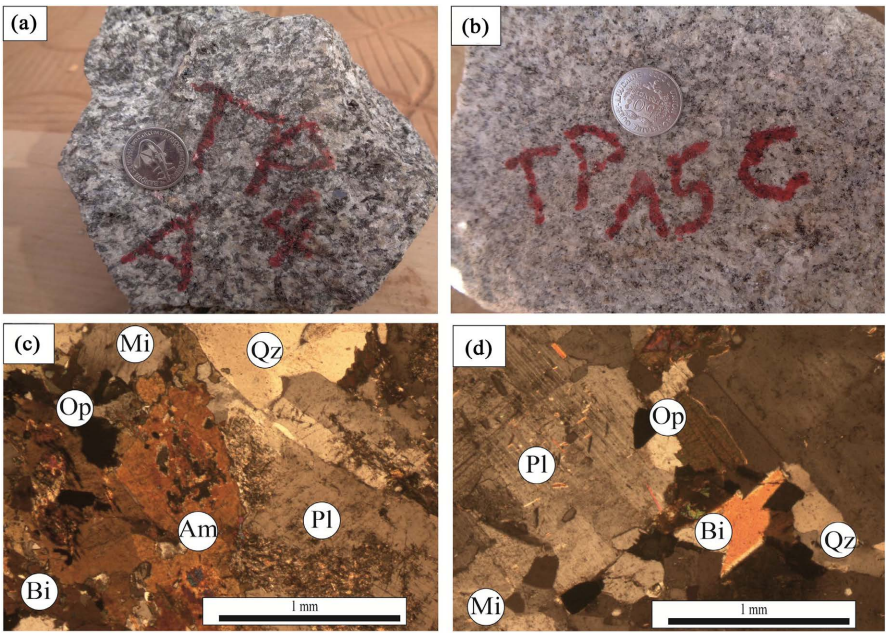

Figure 5. Macroscopic and microscopic view of the granitoids: (a) Granodiorite sample; (b) Biotite granite sample; (c) Microphotograph showing the average mineralogical composition of the granodiorite (polarised and analysed light); (d) Microphotograph showing the average mineralogical composition of the biotite granite (polarised and analysed light): Bi: Biotite, My: Myrmekite, Pl: Plagioclase, Mi: Micrcline, Qz: Quartz, Ep: Epidote.

Table 1. Major elements of basalt and lamprophyre.

Sample	TP 06	TP 07
Pétrography	Lamprophyre	Basalt
Majors elements (%)		
SiO_2	51.7	50.5
TiO_2	0.26	0.99
Al_2O_3	16.05	14.2
Fe_2O_3T	9.39	12.75
MnO	0.16	0.2
MgO	10.15	6.34
CaO	9.83	10.95
Na_2O	2.38	1.86
K_2O	0.15	0.19
P_2O_5	0.06	0.08
Total	100.13	98.06
A/CNK	0.73	0.61

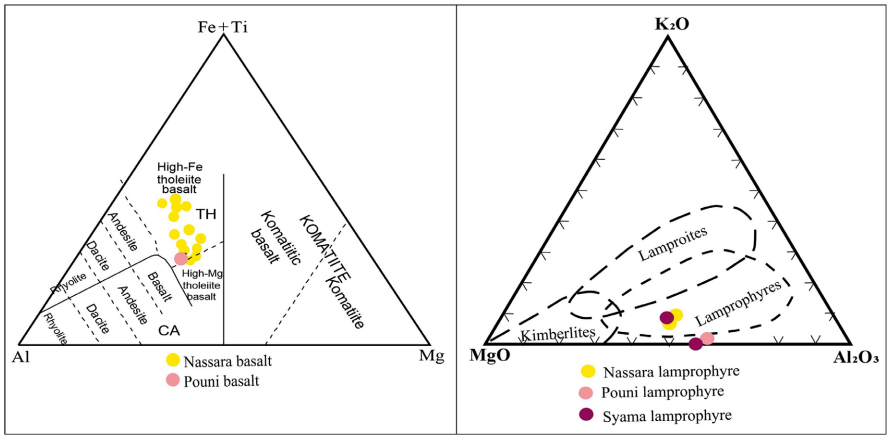

(a) (b)

Figure 6. (a) Position of TP 07 (Pouni basalt) in the AFM ternary diagram; (b) Position of TP 06 (Pouni lamprophyre) in the MgO-Al_2O_3-K_2O ternary diagram.

l'échantillon TP07 a une affinité tholéitique hautement ferrifère et est similaire aux basaltes de Nassara, Houndé et Boromo [9] [10] [12]. Le diagramme MgO-Al_2O_3-K_2O indique que l'échantillon TP06 est un lamprophyre tout comme ceux de Nassara au Burkina Faso et de Syama au Mali (**Figure 6(b)**).

The Zr/Y ratio of sample TP 07 is 2.86 (**Table 2**). According to the Zr/Y ratio defined by [13], the Pouni basalt (sample TP 07) has a tholeiitic affinity like the Nassara basalts [10] and the other Paleoproterozoic basalts of the Man/Leo shield [8].

Table 3 shows the results of the geochemical analysis of samples TP 06 and TP 07.

Table 2. Minor elements of basalt and lamprophyre.

Sample	TP 06	TP 07
Pétrography	Lamprophyre	Basalt
Minors elements (ppm)		
Ba	115.5	46
Rb	2.8	4.1
Sr	544	138
Y	4.7	23.4
Zr	9	67
Nb	0.25	2.9
Th	0.15	0.4
Ga	15.2	18.5
Ti	0.17	0.77
V	180	351
Cr	583	217
Hf	0.25	1.77
Cs	0.24	0.2
Ta	<0.1	1.5
U	<0.05	0.15
W	0.9	<0.5
Sn	<0.5	0.5
Sc	33.4	50.1

Table 3. Traces of basalt and lamprophyre.

Sample	TP 06	TP 07
Pétrography	Lamprophyre	Basalt
REE (ppm)		
La	2.9	4
Ce	6.4	9.9
Pr	0.92	1.6
Nd	3.8	7.2
Sm	0.94	2.55
Eu	0.4	0.88
Gd	0.97	3.73
Tb	0.15	0.58
Dy	0.83	4.16
Ho	0.17	0.88
Er	0.51	2.6

Continued

Tm	0.07	0.38
Yb	0.55	2.61
Lu	0.07	0.39
ΣREE	18.68	41.46
(La/Yb)N	4	1
Eu/Eu*	1.27	0.87

Although we cannot classify sample TP 06, as has been done in other studies [10], we note that its REE spectrum is more or less similar to those of Nassara and Syama in Mali (**Figure 7(a)**). The REE spectrum of sample TP 06 shows an enrichment in light REE compared to heavy REE and a slight positive anomaly less pronounced in Europium (Eu/Eu* = 1.27). This suggests that the spectrum is slightly fractionated with a (La/Yb)N ratio of 4.

The REE spectra in **Figure 7(b)** compare that of sample TP07 with that of the Nassara basalt in Burkina Faso [10]. The REE spectrum of sample TP07 is flat with an insignificant Europium anomaly (Eu/Eu* = 0.87). This is similar to that of the Nassara basalts and suggests that the plagioclases are little or not fractionated.

Condie (1999) [14] define mid-ocean basalts or MORBs (La/Nb > 1.4) and oceanic shelf basalts (La/Nb < 1.4) on the basis of the La/Nb ratio. According to this ratio, sample TP 07 (La/Nb = 1.38 ppm) could be defined as an oceanic shelf basalt.

The negative Ta, Nb and Ti anomalies could define a late orogenic to post-collisional environment for sample TP 06.

4.3.2. Biotite Granites

The geochemical data (**Table 4**) show that the silica content of the granitoids ranges from 60% to 77%, clearly indicating that they are acid rocks. In the molar ratio diagram (A/CNK = $[Al_2O_3]/[CaO] + [Na_2O] + [K_2O]$), the granitoids are type I and are metaluminous to peraluminous (**Figure 8(a)**). In the diagram of [15] the granitoids are calc-alkaline to potassic calc-alkaline (**Figure 8(b)**).

Table 5 shows the average composition of major and minor elements and rare earths in the granitoids of the study area. The evolution of the major elements can be appreciated by correlating their percentages with respect to silica in the different diagrams of [16] of the major elements (**Figures 9(a)-(f)**). As silica increases, elements such as TiO_2, Al_2O_3, MgO and CaO decrease, while Na_2O and K_2O increase. Granitoids are moderately potassic, with the K/Na ratio varying between 0.16 and 0.43.

The REE spectra normalised to the C1 chondrite from [17] show relatively high LREE contents (0.17 < LREE < 38.5) compared to HREE (**Table 6** and **Figure 10(a)**). This reflects a very good fractionation of the REE spectra (**Figure 10(a)**). The (La/Yb)N ratios range from 10 to 26 (**Table 6**) and the Eu anomaly

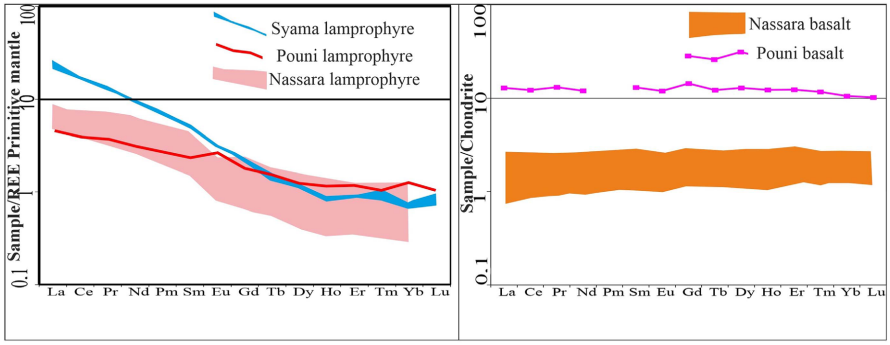

Figure 7. (a) Diagrams of REE normalized to the Primitive mantle for Syama lamprophyre (Mali), Nassara lamprophyre and Pouni lamprophyre; (b) Diagrams of REE normalized to the chondrite C1 for Nassara basalt and Pouni basalt.

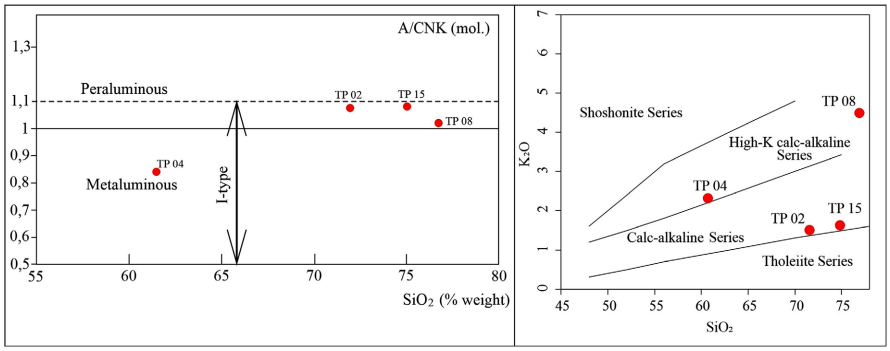

Figure 8. (a) Molar ratio diagrams (A/CNK = $[Al_2O_3]/[CaO] + [Na_2O] + [K_2O]$) of granitoids, (b) Diagram of [15].

Table 4. Major elements of granitoids.

Sample	TP 04	TP 02	TP 08	TP 15
Pétrography	Granodiorite	Biotite granite	Biotite granite	Biotite granite
Majors elements (%)				
SiO_2	60.9	71.8	76.8	74.8
TiO_2	0.63	0.11	0.07	0.11
Al_2O_3	14.75	15.55	12.75	15.35
Fe_2O_3T	6.74	1.64	1.39	1.9
MnO	0.1	0.06	0.05	0.05
MgO	3.68	0.41	0.26	0.44
CaO	5.45	2.78	0.61	2.71
Na_2O	3.22	4.8	3.93	4.65
K_2O	2.3	1.24	4.5	1.4
P_2O_5	0.14	0.05	0.01	0.04
Total	97.91	98.44	100.37	101.45
A/CNK	0.83	1.09	1.02	1.09

Table 5. Minor elements of granitoids.

Sample	TP 04	TP 02	TP 08	TP 15
Pétrography	Granodiorite	Biotite granite	Biotite granite	Biotite granite
Minors elements (ppm)				
Ba	577	717	87.5	851
Rb	86.1	23.2	147.5	28
Sr	418	757	27.9	761
Y	13.1	5.7	11.2	8.7
Zr	135	62	60	77
Nb	5.42	2.54	8.92	2.42
Th	4.66	0.39	7.32	0.7
Ga	16.5	14.6	20.2	14.8
V	158	10	6	9
Ti	0.07	0.4	0.04	0.07
Cr	93	7	11	10
Hf	3.79	1.56	2.81	1.88
Cs	3.77	0.71	0.58	1.13
Ta	0.6	0.6	<0.1	0.1
U	1.06	0.17	1.41	0.33
W	1.3	0.6	0.8	0.8
Sn	1	<0.5	1.3	<0.5
Sc	22	4	6	4.3

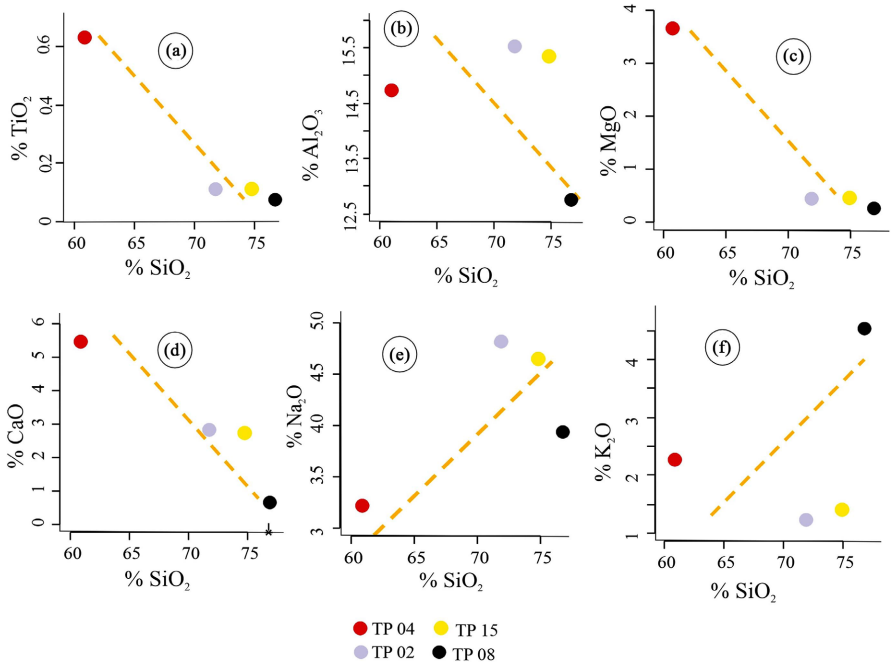

Figure 9. Diagrams of [16] for granitoid majors.

Table 6. Trace elements of granitoids.

Sample	TP 04	TP 02	TP 08	TP 15
Pétrography	Granodiorite	Biotite granite	Biotite granite	Biotite granite
Minors elements (ppm)				
La	18	10.2	10.9	13
Ce	38.5	14	27.7	18.8
Pr	4.69	1.94	3.4	2.63
Nd	17.2	6.1	12	8.8
Sm	3.55	0.99	3.12	1.37
Eu	0.8	0.31	0.17	0.45
Gd	2.8	1.14	2.48	1.44
Tb	0.4	0.15	0.34	0.21
Dy	2.22	0.68	1.86	1.18
Ho	0.49	0.14	0.35	0.28
Er	1.12	0.36	0.95	0.91
Tm	0.18	0.05	0.11	0.11
Yb	1.28	0.32	0.91	0.89
Lu	0.19	0.04	0.11	0.19
ΣREE	91.42	36.42	64.40	50.26
$(La/Yb)_N$	11	26	10	12
Eu/Eu*	0.75	0.89	0.18	0.97

(Eu/Eu* from 0.18 to 0.97) is weakly positive for samples TP 04, TP 02, TP and TP 15. Only sample TP 08 shows a strong negative anomaly. This indicates a good fractionation of the plagioclases. However, the granitoids in the study area are rich in Sr and Ba but poor in Ta and Nb (**Table 2**). These results reflect a good distribution of feldspars and interactions between the different mineral phases.

The multi-element diagrams normalised to EMORB according to [17] are characterised by an enrichment in LILE (Cs, Ba, K, Sr, Nd) compared to HFSE (**Figure 10(b)**). Sample TP 08 has relatively low Ba and Sr contents compared to the other granitoid samples. The profiles are almost parallel and there is a very pronounced anomaly in Ti and moderate anomalies in Nb, Th and P. Overall, these different anomalies depend on the fractionation of potassic minerals, ferromagnesians and plagioclases.

In the geotectonic diagrams of [18], the granitoids of the study area are located in a volcanic arc environment (**Figure 11(a)**) or in the range of syn-plate collision and volcanic arc environment granitoids (**Figure 11(b)**). In the diagram in [19], all the granitoids are located in a volcanic arc environment (**Figure 11(c)**). This shows that they were emplaced in an active tectonic context.

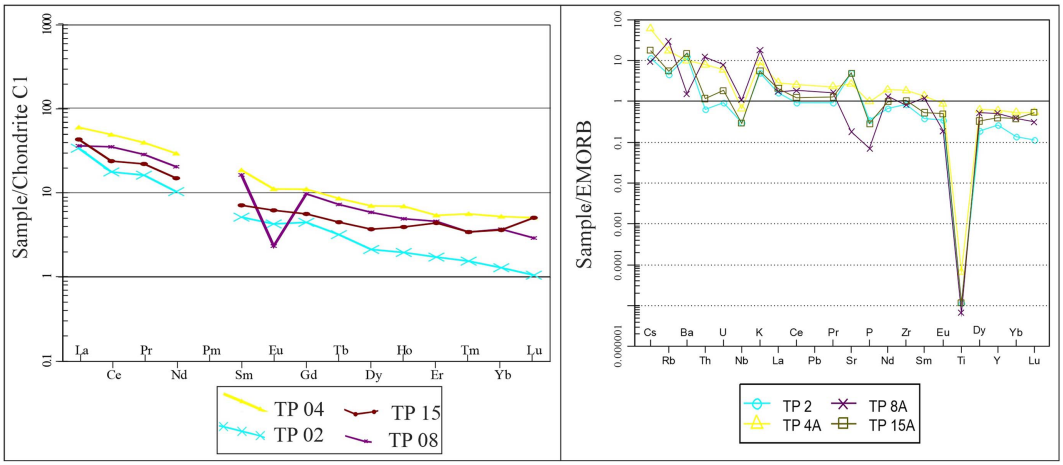

(a) (b)

Figure 10. (a) REE diagrams normalized to the C1 chondrite for the granitoids; (b) Multi-elements diagrams normalized to EMORB for the granitoids.

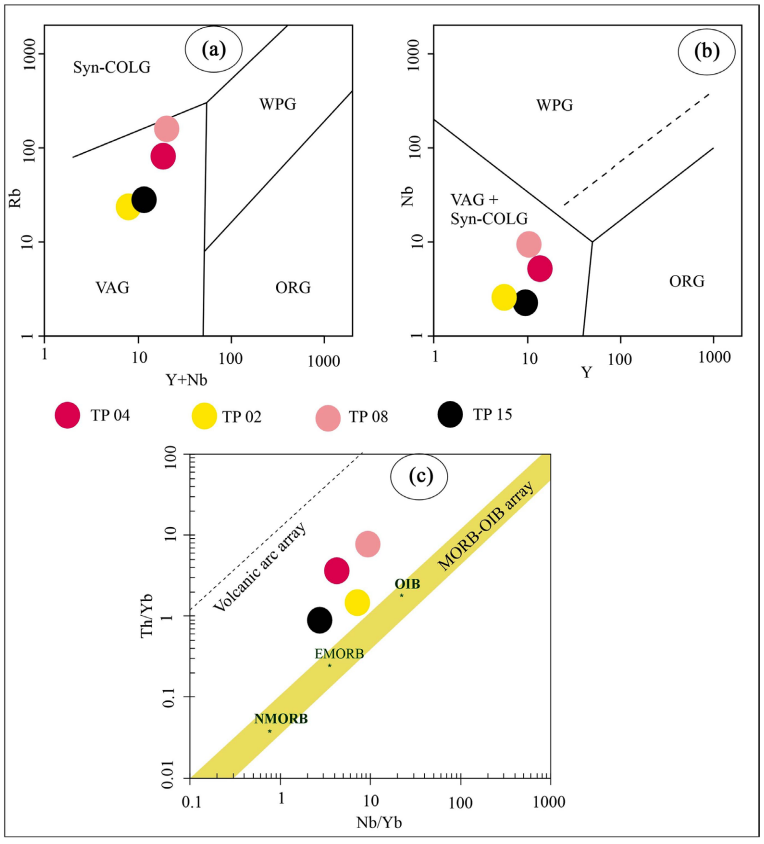

Figure 11. Geotectonic diagrams of granitoids: (a) and (b) Diagram of [18]; (c) Diagram of [19].

5. Discussion

In the study area, the belt rocks identified are basalts and lamprophyres. The granitoids mapped are granodiorites and biotite granites. All these formations, of Paleoproterozoic age, are clearly distinguished by their mineralogical compo-

sitions and geochemical characteristics. The belt rocks are similar to those mapped by [9] in the Houndé and Boromo belts, [10] to the south of the Boromo belt. Rare earth element spectra and minor and trace element contents indicate that the basalts are oceanic plateau basalts, while the lamprophyres are recent dykes and cross-cut the other formations. In the Nassara zone, south of the Boromo belt, these basalts and lamprophyre dykes are mineralised [10] [20].

The granitoids are type I and metaluminous to peraluminous. Rare earth spectra show greater fractionation in the spectra of biotite granites than in granodiorite. Multi-element diagrams normalised to EMORB according to [17] show an enrichment in LILE (Cs, Ba, K, Sr, Nd) compared to HFSE, reflecting good plagioclase fractionation. Similar observations have been made by [1] [4] [21] in Burkina Faso, clearly distinguishing granitoids with a geochemical affinity to Archean TTGs from potassic to highly potassic biotite granites. Based on the different geochemical characteristics of the TTGs, [1] [22] suggest the fusion of basic rocks. Biotite granites, which are much more potassic, are thought to be derived from the partial melting of TTGs [1]. Geotectonic diagrams place the granitoids in a volcanic arc context, but the emplacement mechanisms are different. TTG-type granitoids are emplaced by diapirism in a context of regional shortening [23] [24] [25]. Biotite granites, on the other hand, were emplaced in the context of transcurrent tectonics [4] [26]. In view of the radiometric ages of the granitoids [1] [2] [7] [23] [27]-[34], Yaméogo *et al.* (2020) suggest that the emplacement mechanisms may differ from one locality to another.

6. Conclusion

In the study area, the belt rocks and granitoids are emplaced in different contexts. The basalts are oceanic plateau basalts and the lamprophyres are late. The TTG granitoids, formed by partial melting of the basic rocks, were emplaced in a subduction context. Biotite granites, on the other hand, were probably formed by partial melting of TTGs and emplaced by mechanisms that evolved over time. This suggests that the biotite granites begin to form before the end of the emplacement of the TTGs.

Acknowledgements

This work was a personal project with the support of Professor NABA Séta and associated authors.

Conflicts of Interest

The authors declare no conflicts of interest regarding the publication of this paper.

References

[1] Castaing, C., Billa, M., Milési, J.P., Thiéblemont, D., Le Métour, J., Egal, E., Donzeau, M., Guerrot, C., Cocherie, A., Chèvremont, P., Tegyey, M., Itard, Y., Zida, B.,

Ouédraogo, I., Koté, S., Kaboré, B.E., Ouédraogo, C., Ki, J.C. and Zunino, C. (2003) Notice explicative de la carte géologique et minière du Burkina Faso à 1/1 000 000. Edit. B.R.G.M., Orléans, 147.

[2] Tapsoba, B., Lo, C.-H., Jahna, B.-M., Chunga, S.-L., Wenmenga, U. and Iizuka, Y. (2013) Chemical and Sr-Nd Isotopic Compositions and Zircon U-Pb Ages of the Birimian Granitoids from NE Burkina Faso, West African Craton: Implications on the Geodynamic Setting and Crustal Evolution. *Precambrian Research*, **224**, 364-396. https://doi.org/10.1016/j.precamres.2012.09.013

[3] Tshibubudze, A., Hein, K.A.A. and McCuaig, T.C. (2015) The Relative and Absolute Chronology of Strato-Tectonic Events in the Gorom-Gorom Granitoid Terrane and Oudalan-Gorouol Belt, Northeast Burkina Faso. *Journal of African Earth Sciences*, **112**, 382-418. https://doi.org/10.1016/j.jafrearsci.2015.04.008

[4] Naba, S., Lompo, M., Débat, P., Bouchez, J.L. and Béziat, D. (2004) Structure and Emplacement Model for Late-Orogenic Paleoproterozoic Granitoids: The Tenkodogo-Yamba Elongate Pluton (Eastern Burkina Faso). *Journal of African Earth Sciences*, **38**, 41-57. https://doi.org/10.1016/j.jafrearsci.2003.09.004

[5] Vegas, N., Naba, S., Bouchez, J.L. and Jessell, M. (2008) Structure and Emplacement of Granite Plutons in the Paleoproterozoic Crust of Eastern Burkina Faso: Rheological Implications. *International Journal of Earth Sciences*, **97**, 1165-1180. https://doi.org/10.1007/s00531-007-0205-z

[6] Ilboudo, H., Sawadogo, S., Kagambega, N. and Remmal, R. (2021) Petrology, Geochemistry, and Source of the Emplacement Model of the Paleoproterozoic Tiébélé Granite Pluton, Burkina Faso (Wes-Africa): Contribution to Mineral Exploration. *International Journal of Earth Sciences*, **110**, 1753-1781. https://doi.org/10.1007/s00531-021-02039-3

[7] Doumbia, S., Pouclet, A., Kouamelan, A., Peucat, J.J., Vidal, M. and Delor, C. (1998) Petrogenesis of Juvenile-Type Birimian (Paleoproterozoic) Granitoids in Central Cote-d'Ivoire, West Africa: Geochemistry and Geochronology. *Precambrian Research*, **87**, 33-63. https://doi.org/10.1016/S0301-9268(97)00201-5

[8] Lompo, M. (2009) Geodynamic Evolution of the 2.25-2.0 Ga Palaeoproterozoic Magmatic Rocks in the Man/Leo Shield of the West African Craton. A Model of Subsidence of an Oceanic Plateau. In: Reddy, S.M., Mazumder, R., Evans, D.A.D. and Collins, A.S., Eds., *Palaeoproterozoic Supercontinents and Global Evolution*, Geological Society, London, Special Publication 323, 231-254. https://doi.org/10.1144/SP323.11

[9] Baratoux, L., Metelka, V., Naba, S., Jessell, M.W., Grégoire, M. and Ganne, J. (2011) Juvenile Paleoproterozoic Crust Evolution during the Eburnean Orogeny (~2.2-2.0 Ga), Western Burkina-Faso. *Precambrian Research*, **191**, 18-45. https://doi.org/10.1016/j.precamres.2011.08.010

[10] Ouiya, P., Yaméogo, A.O., Ilboudo, H. and Naba, S. (2022) Implication of Paleoproterozoic Basalt Fertility Related to Mantle Plume Activity in Nassara Gold Mineralization (Burkina Faso, West Africa). *Open Journal of Geology*, **12**, 1013-1031. https://doi.org/10.4236/ojg.2022.1211048

[11] Jenen, L.S. (1976) A New Cation Plot for Classifying Sub-Alkaline Volcanic Rocks. Ontario Division Mines Miscellaneous Paper No. 66.

[12] Augustin, J. and Gaboury, D. (2017) Paleoproterozoic Plume-Related Basaltic Rocks in the Mana Gold District in Western Burkina Faso, West Africa: Implications for Exploration and the Source of Gold in Orogenic Deposits. *Journal of African Earth Sciences*, **129**, 17-30. https://doi.org/10.1016/j.jafrearsci.2016.12.007

[13] Barrett, T.J. and MacLean, W.H. (1999) Volcanic Sequences, Lithogeochemistry, and Hydrothermal Alteration in Some Bimodal Volcanic-Associated Massive Sulfide Systems. In: Barrie, C.T. and Hannington, M.D., Eds., *Volcanics-Associated Massive Sulfide Deposits: Processes and Examples in Modern and Ancient Settings*, GeoScienceWorld, Alexandria, 105-133.

[14] Condie, K.C. (1999) Mafic Crustal Xenoliths and the Origin of the Lower Continental Crust. *Lithos*, **46**, 95-101. https://doi.org/10.1016/S0024-4937(98)00056-5

[15] Peccerillo, A. and Taylor, S.R. (1976) Geochemistry of Eocene Talc-Alkaline Volcanic Rocks from the Kastamonu Area, Northern Turkey. *Contributions Mineralogy Petrology*, **58**, 63-81. https://doi.org/10.1007/BF00384745

[16] Harker, A. (1909) The Natural History of Igneous Rocks. Methuen and Co., London, and Macmillan, New York, 377 p.

[17] Sun, S.S. and McDonough, W.F. (1989) Chemical and Isotopic Systematics of Oceanic Basalts: Implications for Mantle Composition and Processes. In: Sanders, A.D. and Norry, M.J., Eds., *Magmatism in the Ocean Basins*, Vol. 42, Geological Society Special Publication, London, 313-345. https://doi.org/10.1144/GSL.SP.1989.042.01.19

[18] Pearce, J.A., Harris, N.B.W. and Tindle, A.G. (1984) Trace Element Discrimination Diagrams for the Tectonic Interpretation of Granitic Rocks. *Journal of Petrology*, **25**, 956-983. https://doi.org/10.1093/petrology/25.4.956

[19] Pearce, J.A. (2008) Geochemical Fingerprinting of Oceanic Basalts with Applications to Ophiolite Classification and the Search for Archean Oceanic Crust. *Lithos*, **100**, 14-48. https://doi.org/10.1016/j.lithos.2007.06.016

[20] Ouiya, P., Yaméogo, A.O., Sawadogo, S. and Naba, S. (2023) Lamprophyre Rocks in the Nassara Gold Deposit, Southwest Burkina Faso: Characteristics and Implication for Mining Exploration. *Open Journal of Geology*, **13**, 1291-1311. https://doi.org/10.4236/ojg.2023.1312056

[21] Yaméogo, A.O., Naba, S. and Traoré, S.A. (2020) Caractères pétrographiques et géochimiques des granitoïdes de la région de Dori au nord-est du Burkina Faso, Craton Ouest Africain. *Afrique Science*, **16**, 375-395.

[22] Block, S., Baratoux, L., Zeh, A., Laurent, O., Bruguier, O., Jessell, M.W., Ailleres, L., Sagna, R., Parra-Avila, L.A. and Bosch, D. (2016) Paleoproterozoic Juvenile Crust Formation and Stabilisation in the South-Eastern West African Craton (Ghana); New Insights from U-Pb-Hf Zircon Data and Geochemistry. *Precambrian Research*, **287**, 1-30. https://doi.org/10.1016/j.precamres.2016.10.011

[23] Pawlig, S., Gueye, M., Klischies, R., Schwarz, S., Wemmer, K. and Siegesmund, S. (2006) Geochemical and Sr-Nd Isotopic Data on the Birimian of the Kedougou-Kenieba Inlier (Eastern Senegal): Implications on the Paleoproterozoic Evolution of the West African Craton. *South African Journal of Geology*, **109**, 411-427. https://doi.org/10.2113/gssajg.109.3.411

[24] Vidal, M., Gumiaux, C., Cagnard, F., *et al.* (2009) Evolution of a Paleoproterozoic "Weak Type" Orogeny in the West African Craton (Ivory Coast). *Tectonophysics*, **477**, 145-159. https://doi.org/10.1016/j.tecto.2009.02.010

[25] Lompo, M. (2010) Paleoproterozoic Structural Evolution of the Man-Leo Shield (West Africa). Key Structures for Vertical to Transcurrent Tectonics. *Journal of African Earth Sciences*, **58**, 19-36. https://doi.org/10.1016/j.jafrearsci.2010.01.005

[26] Yaméogo, A.O., Ouiya, P., Traoré, A.S., Sawadogo, S., Naba, S., Rousse, S. and Macouin, M. (2023) Rheological Context of Emplacement of the Dori, Gorom-Gorom and Touka Bayèl Granitic Plutons (Northeast Burkina Faso, West African Craton). *Journal of African Earth Sciences*, **208**, Article ID: 105081.

https://doi.org/10.1016/j.jafrearsci.2023.105081

[27] Abouchami, W., Boher, M., Michard, A. and Albarède, F. (1990) A Major 2.1 Ga Old Event of Mafic Magmatism in West Africa: An Early Stage of Crustal Accretion. *Journal of Geophysical Research*, **95**, 17605-17629. https://doi.org/10.1029/JB095iB11p17605

[28] Boher, M., Abouchami, W., Michard, A., Albarède, F. and Arndt, T.N. (1992) Crustal Growth in West Africa at 2.1 Ga. *Journal of Geophysical Research*, **97**, 345-369. https://doi.org/10.1029/91JB01640

[29] Liégeois, J.P., Claessens, W., Camara, D. and Klerkx, J. (1991) Short-Lived Eburnean Orogeny in Southern Mali. Geology, Tectonics, U-Pb and Rb-Sr Geochronology. *Precambrian Research*, **50**, 111-136. https://doi.org/10.1016/0301-9268(91)90050-K

[30] Taylor, N.P., Moorbath, S., Leube, A. and Hirdes, W. (1992) Early Proterozoic Crustal Evolution in the Birimian of Ghana: Constraints from Geochronology and Isotope Geochemistry. *Precambrian Research*, **56**, 97-111. https://doi.org/10.1016/0301-9268(92)90086-4

[31] Gasquet, D., Barbey, P., Adou, M. and Paquette, J.L. (2003) Structure, Sr-Nd Isotope Geochemistry and Zircon U-Pb Geochronology of the Granitoids of the Dabakala Area Cote d'Ivoire: Evidence for a 2.3 Ga Crustal Growth Event in the Palaeoproterozoic of West Africa. *Precambrian Research*, **127**, 329-354. https://doi.org/10.1016/S0301-9268(03)00209-2

[32] Parra-Avila, L.A., Belousova, E., Fiorentini, M.L., Baratoux, L., Davis, J., Miller, J. and McCuaig, T.C. (2016) Crustal Evolution of the Paleoproterozoic Birimian Terranes of the Baoule-Mossi Domain, Southern West African Craton: U-Pb and Hf-Isotope Studies of Detrital Zircons. *Precambrian Research*, **274**, 25-60. https://doi.org/10.1016/j.precamres.2015.09.005

[33] Eglinger, A., Thébaud, N., Zeh, A., Davis, J., Miller, J., Parra-Avila, L.A., Loucks, R., McCuaig, C. and Belousova, E. (2017) New Insights into the Crustal Growth of the Paleoproterozoic Margin of the 185 Archean Kemena-Man Domain, West African Craton (Guinea): Implications for Gold Mineral System. *Precambrian Research*, **292**, 258-289. https://doi.org/10.1016/j.precamres.2016.11.012

[34] Mériaud, N., Thébaud, N., Masurel, Q., Hayman, P., Jessell, M., Kemp, A., Evans, N.J., Fisher, C.M. and Scott, P.M. (2020) Lithostratigraphic Evolution of the Bandamian Volcanic Cycle in Central Cote d'Ivoire: Insights into the Late Eburnean Magmatic Resurgence and Its Geodynamic Implications. *Precambrian Research*, **347**, Article ID: 105847. https://doi.org/10.1016/j.precamres.2020.105847